Available online at www.sciencedirect.com
SCIENCE DIRECT®

Journal of Magnetic Resonance 172 (2005) 231–237

JMR Journal of Magnetic Resonance

www.elsevier.com/locate/jmr

Rapid determination of the RF pulse flip angle and spin–lattice relaxation time for materials imaging

Igor V. Mastikhin*

Department of Physics, MRI Centre, University of New Brunswick, P.O. Box 4400, Fredericton, Canada E3B 5A3

Received 23 August 2004; revised 25 October 2004
Available online 21 November 2004

Abstract

For samples with T_1s longer than 10 s, calibration of the RF probe and a measurement of T_1 can be very time-consuming. A technique is proposed for use in imaging applications where one wishes to rapidly obtain information about the RF flip angle and sample T_1 prior to imaging. The flip angle measurement time is less than 1 s for a single scan. Prior knowledge of the RF flip angle is not required for the measurement of T_1. The resulting time savings in measuring the values of flip angle and T_1 are particularly significant in the case of samples with very long T_1 and short T_2^*. An imaging extension of the technique provides RF flip angle mapping without the need for incrementing the pulse duration, i.e., RF mapping can be performed at fixed RF amplifier output.

Keywords: Long T_1; Short T_2^*; Flip angle; MRI; B_1 mapping; Pure phase encode; SPI; Materials

1. Introduction

Rapid determination of the RF flip angle and the spin–lattice relaxation time, T_1 is highly desirable in an MRI experiment. The RF flip angle and sample T_1 define the level of the signal saturation and thus characterize the image contrast and/or resolution of the MR images [1,2].

Traditionally, one cannot measure T_1 without first calibrating the RF probe, i.e., determining which RF pulse duration will rotate the net magnetization by a required flip angle.

One usually determines the 180°-pulse length by incrementing the pulse duration to find the minimal FID signal or by observing the inversion of the spectral line. The FID acquisition is repeated several times as the RF pulse duration is changed, with a longitudinal magnetization recovery delay of $5T_1$ between the repetitions. If the sample T_1 is long, this method requires a considerable time. One can also apply a train of pulses so that the rotation of the net magnetization can be measured via the pulse nutation frequency [3,4]. However, this method requires that T_2^* be longer than at least n times the probe dead time, where n is the number of pulses applied. Another, more important problem in nutation experiments for samples with $T_1 \gg T_2^*$ is appearance of "nonlinear but periodic distortions" [5] caused by incomplete relaxation. Therefore, for samples with T_2^* lifetimes shorter than hundreds of microseconds, this method is hard to implement.

NMR methods for determination of T_1 can be classified into two groups, "slow" and "rapid" methods, according to their measurement time. In slow methods, such as inversion-recovery, the measurement time of one data scan is determined by the relaxation delay TR and is of order of $5mT_1$, where m is the number of data points in the relaxation curve. In rapid methods such as progressive saturation [6], fast inversion recovery [7], and single-scan methods [8], the measurement time of one data accumulation is of the order of T_1.

* Fax: +1 506 4534581.
E-mail address: mast@unb.ca.

1090-7807/$ - see front matter © 2004 Elsevier Inc. All rights reserved.
doi:10.1016/j.jmr.2004.10.011

The technique proposed here, for rapid determination of RF flip angle and T_1, is a modification of fast single-scan methods. The new technique has advantages in measurement of very long T_1 (>10 s), yielding significant time savings.

I also propose an imaging extension of this technique for RF field mapping. If one is interested in measuring the RF field distribution in a sample with conductive elements, or any sample that produces a significant B_0 shift, frequency-encoding MRI methods will not work well: time evolution artifacts will distort the resulting images [9]. Pure phase encode methods such as SPI (single point imaging) methods are immune to time-evolution image artifacts ([10,11]), and thus should be utilized for RF field mapping in such samples.

One can map the RF field distribution by acquiring a series of images with an increment of the RF pulse duration. This is not always possible in the case of SPI, as the pulses are applied in the presence of magnetic field gradients, and only a part of the sample may be excited. For small RF probes, as utilized for NMR spectroscopy, it is possible to generate very short 180° RF pulses, less than several microseconds in length. For 6–20 cm diameter RF probes that are typically in use for imaging, the duration of the 180° pulse can be several dozens of microseconds. This is too long to ensure broadband sample excitation and therefore one is restricted in the range of useable RF pulse lengths. The proposed technique permits RF field mapping at fixed RF amplifier output, without the need to increment the RF pulse duration.

2. Method

2.1. Measurement of flip angles

The pulse sequence is a train of n RF pulses with flip angle α and the repetition time TR (Fig. 1). In order that transverse magnetization decays completely pulse to pulse, the TR is set so that TR $\gg T_2$ of the sample. In the following discussion we consider solely effects of multiple pulses on longitudinal magnetization.

A single data point is acquired at time t_p after each pulse. The measured signal is

$$S \propto M_z \sin\alpha \exp(-t_p/T_2^*), \tag{1}$$

where M_z is the longitudinal magnetization before the pulse. After n pulses, n data points will be collected. α and t_p are merely scaling factors because they are the same for all n RF pulses, and the evolution of M_z with RF pulsing can be determined.

At time TR after the first RF pulse, the longitudinal magnetization M_z is equal to

$$M_z = M_0 \cos\alpha \exp(-\mathrm{TR}/T_1) + M_0(1 - \exp(-\mathrm{TR}/T_1)). \tag{2}$$

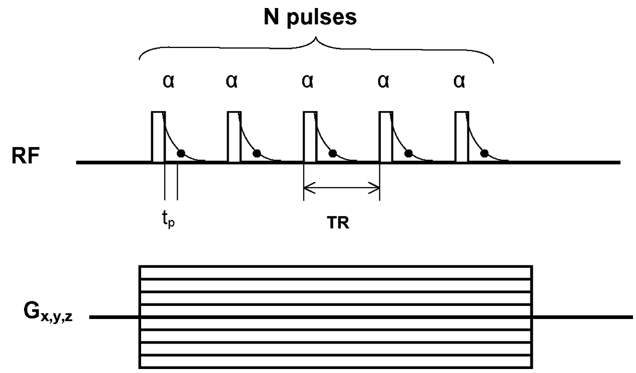

Fig. 1. The pulse sequence for RF flip angle and T_1 measurements is a train of N RF pulses. A single data point is acquired at time t_p after each pulse. In the imaging extension of the sequence, magnetic field gradients are added, similar to an SPI pulse sequence. N RF pulses are applied for each gradient value. N images are acquired which represent the signal decay due to RF pulsing and T_1 relaxation, with the same spatial information.

The longitudinal magnetization M_{zn} after the nth RF pulse is given by Eq. (3) [2,12]:

$$M_{zn} = M_0 C^n E^n + M_0(1 - E)\frac{1 - C^n E^n}{1 - CE}, \tag{3}$$

where $E = \exp(-\mathrm{TR}/T_1)$ and $C = \cos\alpha$. As the number of pulses increases, the value of the longitudinal magnetization approaches a steady-state magnetization

$$M_{st} = M_0 \frac{1 - E}{1 - CE}. \tag{4}$$

Eq. (3) can be rearranged in the following form:

$$\begin{aligned} M_{zn} - M_{st} &= (M_0 - M_{st})\exp(-n\mathrm{TR}/T_1 + n \\ &\quad \times \ln(\cos\alpha)) \\ &= (M_0 - M_{st})\exp(-n\mathrm{TR}/T_{app}), \end{aligned} \tag{5}$$

where T_{app} is defined as [11]

$1/T_{app} = 1/T_1 - \ln(\cos\alpha)/\mathrm{TR}$.

Using the definition of the Ernst angle as $\alpha_E = \mathrm{Arccos}\ \exp(-\mathrm{TR}/T_1)$, Eq. (5) can be rewritten as:

$$\ln\left(\frac{M_{zn} - M_{st}}{M_0 - M_{st}}\right) = -n\frac{\mathrm{TR}}{T_{app}} = n\ln(\cos\alpha\cos\alpha_E) \tag{6}$$

The RF flip angle and the sample T_1 determine the evolution of the longitudinal magnetization towards the steady state. The Ernst angle is a measure of the T_1 impact on the longitudinal magnetization decay for a given TR, in Eq. (6). Information on both the flip angle and T_1 is contained in the product of cosines, $\cos\alpha\cos\alpha_E$. Thus by finding this product, one can extract information on α and T_1.

According to Eq. (6), the longitudinal magnetization decay can be fit to an exponential function $\exp(-kn)$, where n is the number of RF pulses and the decay constant k is:

$$k = \frac{\mathrm{TR}}{T_{\mathrm{app}}} = \frac{\mathrm{TR}}{T_1} - \ln(\cos\alpha) = -\ln(\cos\alpha\cos\alpha_{\mathrm{E}}). \quad (7)$$

An easier way to determine this product of cosines is through observing that the left hand side of Eq. (5) obeys the law of geometrical series. Then

$$\sum_{n=1}^{N}(M_{\mathrm{zn}} - M_{\mathrm{st}}) = \sum \cos^n\alpha\cos^n\alpha_{\mathrm{E}}(M_0 - M_{\mathrm{st}}) = \frac{(1-\cos^N\alpha\cos^N\alpha_{\mathrm{E}})}{1-\cos\alpha\cos\alpha_{\mathrm{E}}}(M_0 - M_{\mathrm{st}}). \quad (8)$$

The sum will be equal to $\frac{(M_0-M_{\mathrm{st}})}{1-\cos\alpha\cos\alpha_{\mathrm{E}}}$ for large N. Therefore, to find the product of cosines, one has to: (1) normalize all the data points to the first data point value M_0; (2) subtract the steady state value M_{st} (the last data point value) from the decay, then sum all points of the decay. This method of determining the product of cosines is less accurate because it does not involve fitting. However, it is very fast and can be applied to an imaging extension of the method for RF field mapping (see below).

The goal of the proposed measurement is to find the flip angle value of a chosen RF pulse length. The value of T_1 is initially unknown, so the Ernst angle is also unknown, and the value of the RF flip angle cannot be extracted from the product of cosines in Eq. (6). However, by setting TR much shorter than T_1, α_{E} can be made very small and the $\cos(\alpha_{\mathrm{E}})$ will be very close to unity. This condition is particularly easy to satisfy in samples with long T_1—the very samples in which conventional methods of determining flip angle are most time consuming. For a range of T_1 between 10 and 50 s (typical of ^{31}P in compact bone), and TR of 10 ms, the range of α_{E} will be from 2.56°–1.14°. The corresponding values of $\cos\alpha_{\mathrm{E}}$ will be between 0.9990 and 0.9998. In this case, the T_1 impact on the magnetization evolution is minimized and $\cos\alpha_{\mathrm{E}}$ can be considered to be unity.

Let us define an ''apparent'' flip angle value α_{A} such that

$$\cos\alpha_{\mathrm{A}} = \cos\alpha\cos\alpha_{\mathrm{E}}. \quad (9)$$

Thus $\alpha_{\mathrm{A}} \cong \alpha$ when $\alpha_{\mathrm{A}} \gg \alpha_{\mathrm{E}}$. For example, for a flip angle of 15° and Ernst angle of 2.56°, as above, the apparent flip angle will be 15.2°.

When the RF flip angle is comparable to the Ernst angle, the apparent flip angle value will deviate from the true RF flip angle value. For example, for T_1 of 10 s and TR of 0.5 s, the Ernst angle will be 17.9°. In this case, the apparent flip angle will be 23.25° when the true flip angle is 15°.

When TR $\ll T_1$, the RF flip angle is the dominant factor in the magnetization decay of Eq. (7), and the apparent flip angle will be very close to the true flip angle. The RF flip angle value can be obtained from a single execution of the pulse sequence. The measurement time, determined by the number of pulses and the repetition time TR, depends on T_1 only if several averages of the data are required to improve the signal-to-noise ratio.

2.2. Measurement of T_1

After the RF flip angle has been determined, one measures T_1 by increasing the TR and repeating the experiment. To find a suitable TR, one may examine the magnetization decay obtained in the flip angle measurement and determine how many pulses were required to bring the signal to the steady state (Eq. (4)). The new TR times this number should be on the order of the expected T_1. After the measurement is performed with the new TR, the T_1 value can be calculated from the Ernst angle contained in the product of cosines (Eq. (6)). T_1 can also be determined from the steady state level, as in progressive saturation, since the RF flip angle has already been determined.

It is also possible to perform T_1 measurements without prior knowledge of the flip angle. In this case, one performs two measurements with the pulse sequence described in the Section 2.1. The flip angle is maintained constant; the pulse repetition time TR is doubled. From Eq. (7), the decay constants for the two measurements will be:

$$\begin{aligned} k_1 &= \mathrm{TR}/T_1 - \ln(\cos\alpha), \\ k_2 &= 2\mathrm{TR}/T_1 - \ln(\cos\alpha), \\ k_2 - k_1 &= \mathrm{TR}/T_1. \end{aligned} \quad (10)$$

The difference between the two decay constants will be TR/T_1. Exact knowledge of the RF flip angle is not necessary; however, the flip angle should be comparable to the Ernst angle for greater accuracy.

The resulting value of T_1 will be correct for signals with one T_1 component and can be used for choosing the sequence parameters for subsequent imaging.

In the general case of P T_1 components, the longitudinal magnetization after the nth pulse will be

$$M_n = \sum_{p=1}^{P}\left[(M_0^p - M_{\mathrm{st}}^p)\exp\left(-\frac{\mathrm{TR}}{T_{\mathrm{app}}^p}n\right) + M_{\mathrm{st}}^p\right]. \quad (11)$$

The signal decay will be multiexponential with the offset equal to the sum of all the steady states. The decay constants and the weighting $(M_0^p - M_{\mathrm{st}}^p)$ can be obtained with multiexponential fitting software such as CONTIN [13]. To find the true weights M_0^p, the steady state values M_{st}^p have to be computed through the use of the corresponding values of T_1^p. However, for shorter T_1 components, the level of the steady state will be higher. The longitudinal magnetization will reach the steady state more rapidly for shorter T_1 components, for which the weights $M_0^p - M_{\mathrm{st}}^p$ will be smaller. This will lead to a reduced accuracy of T_1 measurement for shorter T_1 components.

2.3. Mapping the RF flip angle

An imaging extension of the technique in Section 2.1 permits direct mapping of the RF flip angle for fixed duration excitation pulses. The pulse sequence is identical to the SPI sequence ([10,11]), except for the details of RF excitation. Instead of one pulse per gradient step, a train of N pulses is applied to each gradient step, and one data point is collected at encoding time t_p after each pulse (Fig. 1).

To begin the measurement, the RF probe is filled with a homogeneous sample of known T_1. The choice of RF flip angle and TR for the experiment is determined by two requirements. First, to be the main factor of the magnetization decay, the RF pulse flip angle must be larger than the sample's Ernst angle. Second, the TR should be longer than the sample's T_2 to avoid residual transverse magnetization interference between consecutive pulses. The image data will consist of N images, corresponding to N points of evolution of the longitudinal magnetization.

Both the local RF flip angle and its T_1 counterpart, the Ernst angle, determine the magnetization decay at each pixel. The pixel-by-pixel product of their cosines is calculated either by fitting or, if the signal decays to the steady state by the end of the pulse sequence, by the summation procedure described in Section 2.1, Eq. (8). After the data are divided by $\cos\alpha_E$ at each pixel, the RF flip angle map is obtained.

3. Results and discussion

3.1. Flip angle measurement

The 180°-pulse duration was measured by conventional methods to be 72 μs. A linear dependence of RF flip angle upon pulse duration was assumed to calculate a true flip angle (dashed line on Fig. 2) to the limit of the 180°-pulse measurement (1 μs) and neglecting any nonlinearity imparted by the rise time of the RF amplifier (0.25 μs).

The apparent flip angle values (●, Fig. 2) were derived by fitting the magnetization decays acquired at 23 RF pulse durations.

For given values of the Ernst angle and flip angle, the theoretical values of the apparent flip angle were computed as in Eq. (6) (solid line, Fig. 2). They are in an excellent agreement with the experimentally derived values.

As expected, for longer RF durations the apparent flip angle values are very close to the true flip angle values and change linearly with the pulse duration. When the RF pulse duration approaches the Ernst angle pulse duration (5.5 μs, 13°), the apparent flip angle diverges from the true flip angle. Such behaviour supports our suggestion that extraction of flip angles with the new technique will be accurate for flip angles larger than the Ernst angle.

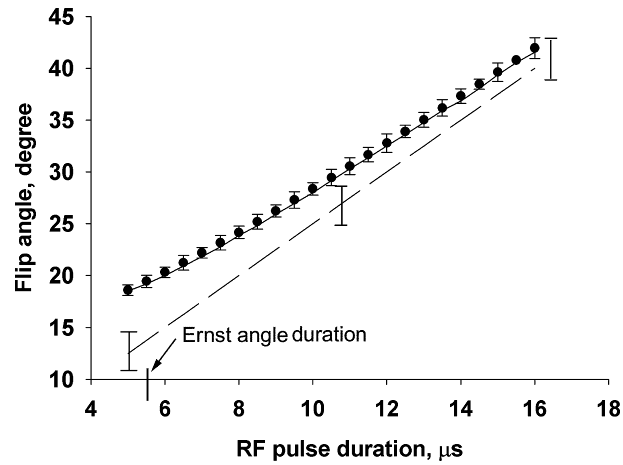

Fig. 2. The experimentally derived, and theoretically calculated, flip angle values vs. RF pulse duration. Apparent flip angle values (●) were derived from decay constants of 23 experimental datasets. The dashed line (– –) represents an assumed linear dependence of true flip angle values on the RF pulse duration, the accuracy shown with error bars. The solid line (–) shows the apparent flip angles calculated as $\alpha_{app} = A\cos(\cos\alpha\cos\alpha_E)$ for a T_1 of 135 ms and TR of 4 ms. As the RF pulse duration approaches the Ernst angle duration of 5.5 μs, T_1 effects surpass flip angle effects, and the apparent flip angle exceeds the true flip angle.

This method was employed to calibrate a ^{7}Li probe in the case of a solid sample with long T_1. The sample was a loose pack of LiF crystals. The sample T_2^* of 47 μs did not permit using pulse nutation methods to calibrate the RF probe. Before measuring T_1, the pulse sequence with a TR of 10 ms was executed to find the flip angle corresponding to an RF pulse duration of 4 μs. The LiF sample was expected to have a T_1 of approx. 30 s, so the Ernst angle for such parameters was estimated to be 1.4°. Therefore, the T_1 impact on the magnetization decay, Eq. (6), was expected to be very small, and the apparent RF flip angle was expected to be very close to the true flip angle.

An RF flip angle of 18.5° was extracted from the signal decay constant. The measurement itself took 1.28 s. If one tried to determine the RF flip angle by seeking the 180°-pulse, the measurement time would b $5T_1M$, where M would be a number of trials with different pulse durations. To determine the flip angle correctly, the number of trials would have to be more than 10, otherwise the precision of the calibration would be compromised. For the ^{7}Li sample T_1 of 50 s (see below), the measurement time would be longer than $5 \times 50 \times 10 = 2500$ s. One can see clear advantages of the proposed technique.

This RF pulse duration ($\alpha = 18.5°$) was utilized in subsequent measurements of T_1 at TR delays of 1, 2, and 4 s.

3.2. Measurement of T_1

^{7}Li signal data from a LiF crystalline sample are shown in Fig. 3. The four datasets were acquired at TRs of 10 ms, 1, 2, and 4 s, with steady-state offset subtracted. The decay constants for experiments with a TR of 1 and 2 s were found. They were subtracted, Eq. (10), yielding a T_1 of 51 ± 4 s. The same procedure, with a TR of 2 and 4 s, resulted in a T_1 of 52 ± 4 s. Thus no prior information on the RF flip angle was necessary for T_1 measurement. Independently, a value was also calculated for three data decays using the known value of the flip angle as in Eq. (6). T_1 was found to be the same within experimental precision. The acquisition time was determined by the number of pulses 64 and the chosen TR. The acquisition time was 1, 2, and 4 min for TRs of 1, 2, and 4 s respectively.

As is clear in Fig. 3, the signal reached a steady state after 40–50 pulses. The steady state levels were used for another independent measurement of the T_1, this time via the progressive saturation method. The "steady state" T_1s were 44 ± 4, 43 ± 4, and 47 ± 4 s for TRs of 1, 2, and 4 s.

The observed differences between the T_1 values obtained with our technique and through the progressive saturation are small but not negligible. It is possible that the strong coupling between the two magnetic nuclei, Li and F in the crystal will cause magnetization exchange thus changing the measured T_1 [14].

In the case of a strong magnetization exchange on the timescale of our measurement [15], additional mechanisms will cause magnetization loss so the proposed technique will not be applicable.

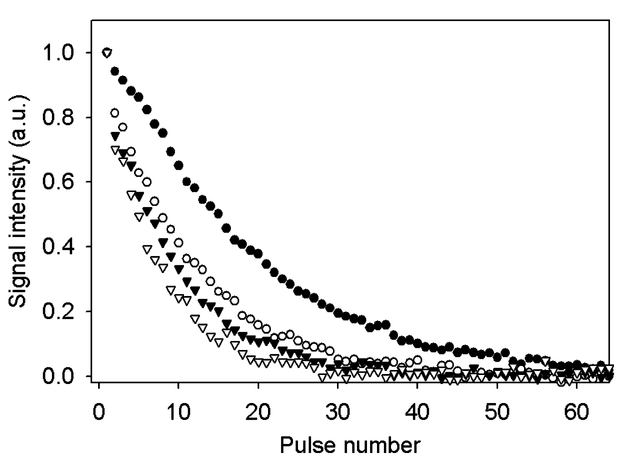

Fig. 3. Normalized ^{7}Li signal versus pulse number for a TR of 10 ms (●), 1 s (○), 2 s (▼), and 4 s (▽). A single data point is acquired after each of 64 RF pulses. The flip angle was 18.5°. There was no signal averaging. A longer TR increases the T_1 effect on the magnetization decay. The measured T_1 was 51 ± 4 s; the measurement time was 2 min for a TR of 2 s.

3.3. Mapping the RF flip angle

The imaging extension of the technique (Fig. 1) was applied to mapping the flip angle distribution in a plane parallel to a 10 mm diameter circular surface coil at a distance of 2 mm. A thin sheet of rubber was positioned on top of the surface coil. The flip angle distribution (Fig. 4) was calculated from a dataset of 16 images. The radius of the signal area is very close to the radius of the surface coil, as expected, with the maximum of the signal at the centre.

An interesting feature of the flip angle map is the elliptical shape of the RF field from the circular surface coil. This is a well-known feature of the RF field distribution near a circular surface coil (see, for example, [16,17]). The plane of the coil was parallel to the B_0 field direction. The NMR signal will be excited only by B_1 field components that are orthogonal to B_0. The principal source of sample excitation is the B_1 *Y*-component orthogonal to the plane of the coil. However, the flux of the B_1 field diverges at the edges of the coil where two other B_1 components, *X* and *Z* are also significant. The *Z*-component is parallel to B_0, hence does not excite the sample. The *X*-component, however, is orthogonal to B_0 and will excite the sample, causing the observed elongation of the flip angle map.

After the first measurement above, a 0.3 mm thick, 15 mm long straight piece of copper wire was placed across the centre of the rubber sample and a new measurement, with the same parameters, was performed. A new flip angle distribution (Fig. 5) was calculated from the dataset. Changes in the RF field distribution are noticeable: the high signal area is now split in two, the centre of the splitting coincides with the wire position. This was expected, because the RF field will be reduced near the conductive element and the RF flip angle will be decreased near the wire. A simulation of the RF

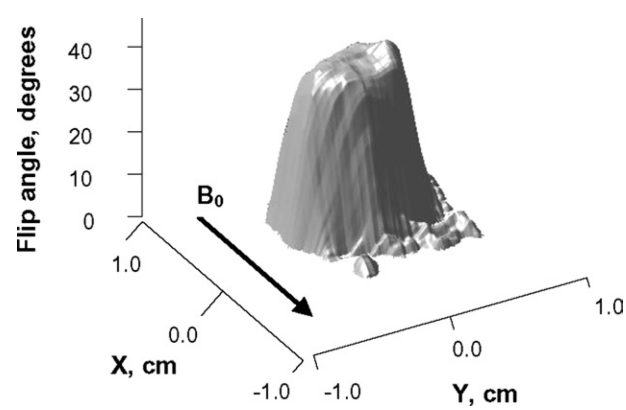

Fig. 4. The surface-shaded plot of the flip angle map for a 0.3 mm thick, 20 mm square rubber sample positioned 2 mm from a 1 cm circular surface coil. The vertical axis is calculated to be the flip angle in degrees. The *X* and *Y* axes are spatial coordinates. The B_0 field is directed along the *X* axis, in this figure.

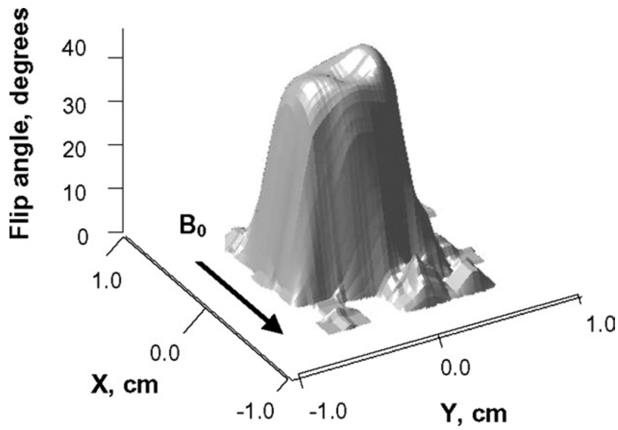

Fig. 5. The surface-shaded plot of the flip angle map for the same rubber sample as in Fig. 4 with a 0.3 mm thick copper wire placed on top. The high signal area is split in two due to the reduction of the RF field in the vicinity of the wire.

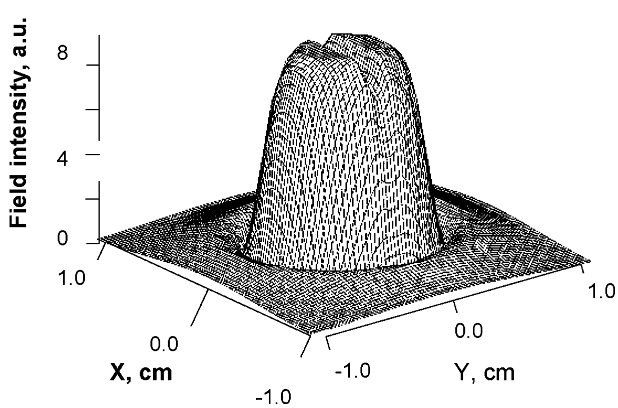

Fig. 6. A simulated flip angle map for the rubber sample with a 0.3 mm-thick, 15 mm-long straight wire atop. A similar splitting as in Fig. 5 is present.

field distribution around the surface coil, with the wire in place, is shown in Fig. 6. A similar splitting due to shielding of the RF field is observed.

4. Conclusion

A technique is proposed for use in imaging applications where there is a need to quickly determine the flip angle and T_1 of the sample prior to imaging. The resulting time savings in measuring the values of flip angle and T_1 can be significant in the case of samples with very long T_1 and short T_2^*.

For flip angle measurements with the proposed methodology, the acquisition time is equal to $n * \mathrm{TR}$ where n is the number of RF pulses, and is less than a second for a single signal average. By comparison, techniques for measuring the flip angle such as 180-pulse determination, require several data acquisitions with the recovery delay of 5 T_1s making the measurement of order of an hour for samples with $T_1 \sim 1$ min.

Measurements of T_1 do not require prior knowledge of the RF flip angle with this technique. One drawback is the lower dynamic range of the measurement compared to conventional methods, since flip angles less than 90° or 180° are employed.

The imaging extension of the technique provides RF flip angle mapping without the need for incrementing the pulse duration: RF mapping can be performed at fixed RF amplifier output. This is important for measurements of heterogeneous conductive samples such as aircraft wings [9] where eddy currents generated by the RF pulse will depend on the duration of the pulse, and where conventional frequency-encode imaging methods fail. This may also be important in measuring the RF field distribution in conductive structures such as guide wires and catheters in interventional MRI [18].

5. Experimental

All experiments were performed on a Nalorac (Martinez, CA) 2.35 T 32 i.d. horizontal bore superconducting magnet, with a Tecmag (Houston, TX) Apollo console. A water-cooled 7.5 cm-id Nalorac gradient set driven by Techron (Elkhart, IN) 8710 amplifiers, was employed. ^{1}H (100 MHz) and ^{7}Li (38.8 MHz) measurements were performed using home-made eight-rung birdcage coils driven in quadrature by a 2-kW AMT (Brea, CA) 3445 RF amplifier with a rise time of 0.25 μs. Image processing was performed with Interactive Data Language 6.0 (Research Systems, Boulder, CO).

For flip angle measurements, a cross-linked *cis*-polybutadiene disk of 4 cm diameter and 0.8 cm thickness was used, with relaxation parameters $T_1 = 138$ ms, $T_2^* = 350$ μs. The 180°-pulse length was 72 ± 1 μs. The Ernst angle was 13° for the *cis*-polybutadiene disk, which corresponded to a pulse length of 5.5 μs. The pulse sequence of Fig. 1, with gradients off, was used with 128 RF pulses, TR = 4 ms, and four signal averages. A single data point was acquired 20 μs after each pulse. The recovery delay between pulse trains was 0.5 s. The measurement was performed for 23 values of the RF pulse duration, incremented in 0.5 μs steps, from 5 to 16.5 μs. The decay constants k were determined from the magnetization decays as described in Section 2.1. Both exponential fitting and the geometric series summation generated the same (within 6%) decay constant values. The fitting was performed with an IDL fitting routine. The apparent flip angle was calculated for each of the 23 measurements.

An LiF crystalline sample was employed for T_1 measurements. Four datasets were acquired at TRs of 10 ms, 1, 2, and 4 s, each with no signal averaging. The RF pulse duration was maintained at 4 μs.

For RF flip angle mapping, a 0.2 mm thick 20×20 mm square rubber sheet was positioned above a circular surface coil. The coil diameter was 10 mm, the coil to rubber distance was 2 mm. The rubber T_1 was 130 ± 8 ms, with T_2^* equal to 0.7 ± 0.1 ms. Imaging parameters were as follows: encoding time t_p of 120 μs, 64×64 imaging matrix with maximum gradient of 28 G/cm and nominal isotropic resolution of 0.34 mm. For flip angle mapping, 16 RF pulses were applied with a single data point acquired at time t_p after the pulse for each gradient step, with a 4 μs pulse duration and a 4 ms interval between the pulses.

The acquired data formed a $16 \times 64 \times 64$ matrix with the first dimension of 16 points corresponding to the longitudinal magnetization evolution during RF pulsing. The matrix was split into 16 separate *k*-space data sets and Fourier transformed.

To eliminate the background noise in the flip angle map, the pixels with high intensity were masked. All 16 images were added; only points with intensities above a threshold value were selected for the flip angle mapping procedure. The product $\cos\alpha\cos\alpha_E$ was calculated from images via the geometric series summation. The flip angle values were obtained after dividing the product by the $\exp(-TR/T_1)$ factor to remove the T_1 relaxation component. The resulting flip angle map was plotted as a surface map, with spatial dimensions as X and Y, with flip angle values plotted on the axis Z of the map. The B_0 field is directed along the X-axis in this figure.

After the first measurement, a 0.3 mm thick 15 mm long copper wire was placed atop the sample, and the procedure was repeated with the same parameters as before. With four signal averages, the total imaging time was 65 min.

The RF field distribution around the surface coil was simulated with Microwave Studio 4.0 (Computer Simulation Technology, Darmstadt, Germany) Finite Integration Method based software package. The magnetic field B_0 is parallel to the plane of the 10 mm circular surface coil. The intensity of the image corresponds to the flip angle of RF field components orthogonal to B_0 at the height of 2 mm.

Acknowledgments

I.V.M. thanks Ben Newling and Bruce Balcom for useful discussions, Rod McGregor for motivating the work. I.V.M. also thanks NSERC of Canada for an operating grant and a Major Facilities Access award to the UNB MRI Centre. Andrew Marble's work simulating the RF field distribution is greatly appreciated.

References

[1] A. Haase, J. Frahm, D. Matthaei, W. Hänicke, K.-D. Merboldt, FLASH imaging. Rapid NMR imaging using low flip-angle pulses, J. Magn. Reson. 67 (1986) 258–266.
[2] I.V. Mastikhin, B.J. Balcom, P.J. Prado, C.B. Kennedy, SPRITE MRI with prepared magnetization and centric *k*-space sampling, J. Magn. Reson. 136 (1999) 159–168.
[3] K.R. Metz, J.P. Boehmer, J.L. Bowers, J.P. Moore, Rapid rotating-frame imaging using an RF pulse train (RIPT), J. Magn. Reson. B 103 (1994) 152–161.
[4] D. Canet, Radiofrequency field gradient experiments, Progr. NMR Spectrosc. 30 (1997) 101–135.
[5] K.I. Momot, N. Binesh, O. Kohlman, C.S. Johnson, Toroid cavity detectors for high-resolution NMR spectroscopy and rotating frame imaging: capabilities and limitations, J. Magn. Reson. 142 (2000) 348–357.
[6] R. Freeman, H.D.W. Hill, Fourier transform study of NMR spin–lattice relaxation by "progressive saturation", J. Chem. Phys. 14 (1971) 3367–3377.
[7] D. Canet, G.C. Levy, I.R. Peat, Time saving in ^{13}C spin–lattice relaxation measurements by inversion-recovery, J. Magn. Reson. 18 (1975) 199–204.
[8] R. Kaptein, K. Dijkstra, C.E. Tarr, A single-scan Fourier transform method for measuring spin–lattice relaxation times, J. Magn. Reson. 24 (1976) 295–300.
[9] A.E. Marble, I.V. Mastikhin, R.P. MacGregor, M. Akl, G. LaPlante, B.G. Colpitts, P. Lee-Sullivan, B.J. Balcom, Distortion-free single point imaging of polymer-metal composite aircraft control surfaces, J. Magn. Reson. 168 (2004) 164–174.
[10] S. Emid, J.H.N. Creyghton, High resolution NMR imaging in solids, Phys. B 128 (1985) 81–83.
[11] S. Gravina, D.G. Cory, Sensitivity and resolution of constant-time imaging, J. Magn. Reson. B 104 (1994) 53–61.
[12] M.T. Vlaadingerbroek, J.A. den Boer, in: Magnetic Resonance Imaging, Springer, Berlin, 1996, p. 218.
[13] S.W. Provencher, CONTIN—a general-purpose constrained regularization program for inverting noisy linear algebraic and integral-equations, Comput. Phys. Commun. 27 (1982) 229–242.
[14] V.E. Zobov, A.A. Lundin, O.E. Rodionova, The shape of NMR absorption and cross-relaxation spectra in a heteronuclear spin system, J. Exp. Theor. Phys. 93 (2001) 542–557.
[15] R.G.S. Spenser, K.W. Fishbein, Measurement of spin–lattice relaxation times and concentrations in systems with chemical exchange using the one-pulse sequence: breakdown of the Ernst model for partial saturation in nuclear magnetic resonance spectroscopy, J. Magn. Reson. 142 (2000) 120–135.
[16] D.I. Hoult, B. Tomanek, Use of mutually inductive coupling in probe design, Concepts Magn. Reson. 15 (2002) 262–285.
[17] A.V. Ouriadov, R.P. MacGregor, B.J. Balcom, Thin film MRI-high resolution depth imaging with a local surface coil and spin echo SPI, J. Magn. Reson. 169 (2004) 174–186.
[18] W.R. Nitz, A. Oppelt, W. Renz, C. Manke, M. Lenhart, J. Link, On the heating of linear conductive structures as guide wires and catheters in interventional MRI, J. Magn. Reson. Imaging 13 (2001) 105–114.